Spectrochimica Acta Part B: Atomic Spectroscopy 208 (2023) 106779

Contents lists available at ScienceDirect

Spectrochimica Acta Part B: Atomic Spectroscopy

journal homepage: www.elsevier.com/locate/sab

Assessment of total sample consumption infrared-heated system for minimization of matrix effects in ICP-tandem mass spectrometry

Raquel Sánchez *, José-Luis Todolí

Department of Analytical Chemistry, Nutrition and Food Sciences, University of Alicante, 03690 San Vicente del Raspeig, Alicante, Spain

ARTICLE INFO

Keywords:
Total sample consumption infrared-heated system (IR-TSC)
ICP-MS/MS
Metal content
Matrix effect
Polyatomic interferences

ABSTRACT

A total sample consumption infrared-heated system (IR-TSC) has been coupled to ICP-tandem mass spectrometry (ICP-MS/MS) for the first time. The objective of this study was to assess the analytical performance of the IR-TSC system, in terms of analytical figures of merit and mitigation of matrix effects. Twenty-seven elements have been determined: Ag, Al, As, B, Ba, Be, Bi, Cd, Co, Cr, Cu, Fe, K, Li, Mn, Mo, Ni, Pb, Rb, Sb, Se, Sn, Sr, Ti, Tl, V and Zn. Different operating conditions, including nebulization flow rate and spray chamber temperature, were optimized to improve sensitivity, signal stability, and plasma thermal conditions. The results showed that the infrared-heated sample introduction system improved the signal intensity by a factor of 2 to 4 compared to a conventional sample introduction system, whereas the limits of detection (LODs) improved by a factor going from 1.2 (Ba) to 3.3 (Cr) for a sample containing 2% HNO_3. Meanwhile, for a 10% ethanol sample the improvement factor ranged from 1.4 (Ti) to 3.8 (Cr). Matrix effects for solutions containing inorganic acids or high content of sodium (2% HNO_3, 10% HNO_3, 20% HNO_3, 10% HCl; 500 mg kg^{-1} Na, 500 mg kg^{-1} Na + 10% HNO_3) were mitigated under optimum conditions (IR-TSC at 125 °C). Meanwhile, for solutions containing organic solvents (10% ethanol, 10% acetic acid, and 10% formic acid) it was not possible to eliminate matrix effects, even when applying an internal standard. For Se and As, elements spectrally interfered, the combination of IR-TSC sample introduction system with oxygen as reaction/collision gas mode in ICP-MS/MS provided accurate results. For 10% HNO_3 and 10% HCl relative intensities values, calculated taking the signal intensity obtained for 2% HNO_3 as reference, were close to the unity. Environmental and clinical control and certified reference materials were analyzed by means of an external calibration approach, with most of the elements showing concentrations not significantly different from the certified values. Finally, the IR-TSC was tested on twelve real samples, including seawater, surface water, peritoneal fluid, seminal plasma, wine, and bioethanol samples, demonstrating the system potential in different application fields.

1. Introduction

Inductively coupled plasma-mass spectrometry (ICP-MS) is widely recognized as the most powerful analytical technique for determining the concentration and isotopic composition of a wide range of elements in diverse sample matrices, including environmental, biological, clinical and industrial matrices [1]. ICP-MS is renowned for its exceptionally low detection limits at the parts-per-trillion level, good precision, wide dynamic range, and robustness. Nevertheless, the accuracy of this technique remains a significant concern due to potential spectroscopic and non-spectroscopic interferences that can arise from the sample matrix [2–5]. Interferences resulting from the presence of atomic or molecular ions with identical mass-to-charge ratio as the analyte ion could be effectively minimized by implementing matrix separation, alternative sample introduction systems, modified plasmas or systems equipped with collision/reaction cells (CRC) [6]. An effective way to minimize polyatomic interferences is through the use of ICP-tandem mass spectrometry (ICP-MS/MS) [7], [8]. The main difference with a traditional ICP-MS is the integration of an extra quadrupole before the collision/reaction cell (CRC), working as a mass filter. As a result, only ions with a specific *m/z*-ratio are permitted to access the CRC, leading to more precise management of reactions inside the cell [7,8].

Non-spectroscopic interferences are strongly influenced by the nature and concentration of the sample matrix, as well as the instrument and operating conditions [5]. Several mechanisms have been proposed to explain the matrix effects, including variations in the mass of solvent

* Corresponding author.
E-mail address: r.sanchez@ua.es (R. Sánchez).

https://doi.org/10.1016/j.sab.2023.106779
Received 20 March 2023; Received in revised form 19 July 2023; Accepted 19 August 2023
Available online 20 August 2023

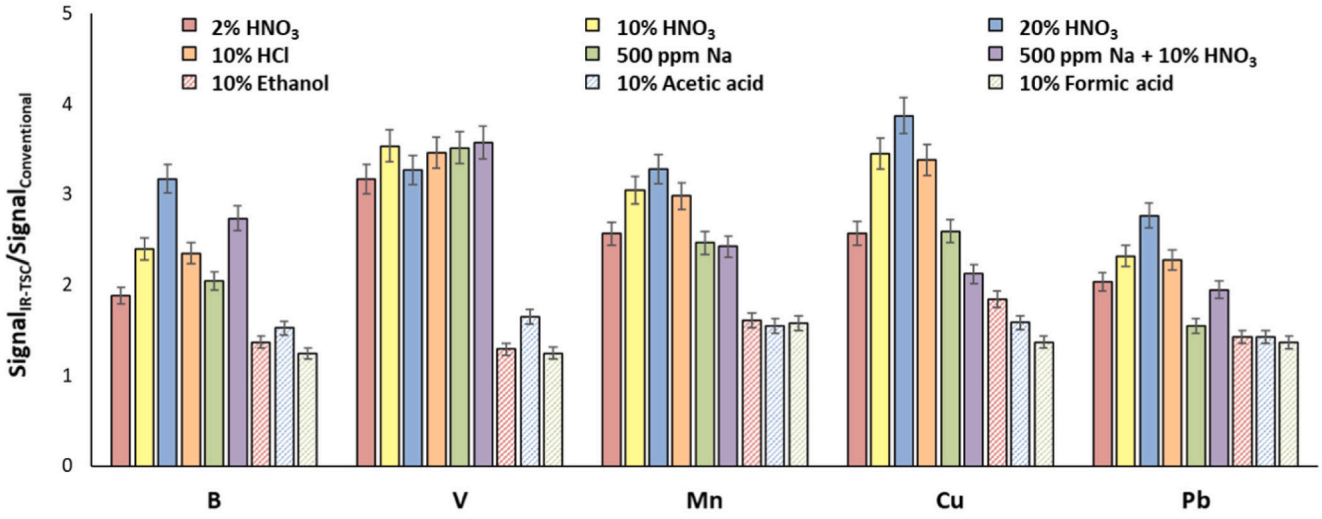

Fig. 1. Signal intensity (mean ± standard deviation) for IR-TSC at 125 °C heating temperature divided by that for the conventional sample introduction system for the different matrices evaluated. Experimental operating conditions described in Table S2 (Appendix). Analyte concentration: 50 μg kg^{-1}. Number of replicates: 5. Errors bars: standard deviation.

and analyte delivered to the ICP, shift in the ionization equilibrium; enhanced ionization by charge transfer reactions and secondary discharges; loss of analyte ions through lateral and ambipolar diffusion, space-charge effects and collisional scattering; deposition of dissolved solids on the nebulizer and torch injector tips, and interface cones [5,9].

Changes in physical properties of the sample solution could modify the aerosol characteristics, thus modifying solvent and analyte transport efficiency when using pneumatic nebulization [10–16]. On this subject, the spray chamber is recognized as one of the most significant sources of matrix effects [17]. One possible solution is to replace the conventional sample introduction system by alternative heating systems based on infrared radiation (IR) sources. Up to date, the infrared radiation heating has been applied to single-pass flip chamber (FC), double-pass, or cyclonic spray chambers coupled to ICP-OES [18–22], or ICP-MS [23,24]. Similarly to the observations made for conduction and convection heating [25], IR-based heating systems enhance the analytical performance of ICP techniques in terms of sensitivity, detection limit, plasma robustness, and precision [18–24].

Up to now, the infrared radiation heating system has been employed to analyze aqueous samples by ICP-OES and ICP-MS. Nevertheless, the application of the IR heated sample introduction system has never been explored with organic matrices. The goal of the present work was thus to evaluate the analytical performance of the combination of the total sample consumption infrared-heated system (IR-TSC) for ICP-MS/MS. Analytical figures of merit were compared with those for a conventional sample introduction system. In addition, a systematic evaluation of matrix effects was conducted for the first time, including solutions containing inorganic acids, high concentrations of sodium, and solutions containing organic solvents. Twenty-seven analytes were determined, including spectrally interfered nuclides such as ^{75}As and Se isotopes.

2. Experimental

2.1. Reagents and samples

10 mg L^{-1} multi-element standard, SCP33MS (SCP Science, Quebec, Canada) was used as stock solution. Standards were prepared daily by serial dilution in ultrapure water (Millipore, El Paso, TX, USA). The analyte concentrations ranged from 0.05 to 250 μg L^{-1}. A solution containing four internal standard (IS) elements (Ge, Sc, Rh and Re) (SCP SCIENCE) was continuously delivered and on-line mixed with the liquid sample stream. Internal standards final concentration was 40 μg L^{-1}.

65% HNO_3 and 37% HCl (Suprapur, Merck, Darmstadt, Germany) were used for the preparation of acid matrices for the study of matrix effects. Sodium nitrate (Panreac, Barcelona, Spain) was used for the preparation of salty matrices. Ethanol, acetic acid, and formic acid were used as organic matrices (Panreac, Barcelona, Spain). For the optimization of critical variables, a multi-elemental 50 μg L^{-1} solution prepared in 2% HNO_3 was used. In order to evaluate matrix effects, different solutions were prepared (percentages in *w*/w): 2% HNO_3, 10% HNO_3, 20% HNO_3, 10% HCl; 500 mg kg^{-1} Na, 500 mg kg^{-1} Na + 10% HNO_3, 10% ethanol, 10% acetic acid and 10% formic acid. A portion of the different matrix solutions was spiked with a multi-elemental 50 μg L^{-1} solution.

Three seawater certified reference samples and two clinical control samples were analyzed in the present work. The characteristics of the certified and control samples are shown in Table S1 (Appendix).

2.2. Instrumentation

Ionic intensities were measured by using an Agilent 8900 ICP-QQQ instrument (Agilent Technologies, CA, USA). This instrument is equipped with an octopole collision-reaction cell (CRC) located in-between two quadrupole analyzers. Two cell modes (no gas and He mode) were selected. The sample introduction system was a glass pneumatic concentric nebulizer (TR-30-A1, Meinhard® Glass Products, Santa Ana, USA) and an infrared-heated total sample consumption introduction system (IR-TSC), equipped with a 47 cm^3 single-pass spray chamber (Fig. S1 (Appendix)). The infrared heating source corresponded to two lamps emitting light at a wavelength range going from 0.5 to 5 μm (Fig. S1 (Appendix)). The solutions were delivered in continuous sample aspiration mode to the nebulizer by means of a peristaltic pump Perimax 16 antipuls, (Spetec GmbH, Erding, Germany) and a 0.25 mm flared end PVC tubing (Glass Expansion, Melbourne, Australia). A conventional double-pass spray chamber cooled at 5 °C coupled to a pneumatic concentric nebulizer was taken as the reference system. The operating conditions are summarized in Table S2 (Appendix).

3. Results and discussion

The analytical performances of the infrared-heated total sample consumption system (IR-TSC) in combination with an ICP-MS/MS were assessed with samples containing different matrices. In a first step, a systematic optimization was done in terms of net signal intensity (I_{net})

Table 1
Limits of detection (ng L^{-1}) for IR-TSC at 125 °C heating temperature and the conventional sample introduction system. Sample matrices: 2% HNO_3 and 10% ethanol.

		Ag	Al	As	B	Ba	Be	Bi	Cd	Co	Cr	Cu	Fe	K	Li	Mn	Mo	Ni	Pb	Rb	Sb	Sn	Sr	Ti	Tl	V	Zn
2% HNO_3	*IR-TSC*	5	6	23	13	10	10	9	4	13	16	13	53	8	8	1.2	10	12	3	8	10	3	4	12	3	4	9
	Conventional	14	14	39	33	12	18	24	10	18	54	29	151	20	17	2	31	18	6	20	20	5	12	18	5	6	24
10% Ethanol	*IR-TSC*	8	9	28	14	11	15	12	6	13	13	15	51	13	13	2	14	14	4	11	12	5	9	14	4	7	8
	Conventional	18	15	47	28	19	22	28	11	21	50	31	78	22	19	4	33	19	7	21	28	8	15	19	7	11	21

(Eq. 1).

$$I_{net} = I_{Spiked\ sample} - I_{Blank\ solution} \quad (1)$$

where $I_{Spiked\ sample}$ and $I_{Blank\ solution}$ were the signal intensities of the spiked and non-spiked matrix solutions, respectively. The liquid flow rate was set at 30 μL min^{-1}, as the IR-TSC has been designed to operate at very low liquid flow rates. The critical variables studied were the nebulizer gas flow rate as well as the IR-TSC chamber temperature. Plasma thermal stability was evaluated by measuring $^{36}Ar^+$ signal intensity, $^9Be/^7Li$ and oxide ratios. Then, the developed sample introduction system was compared with a conventional cooled double-pass spray chamber in terms of signal intensity, limit of detection and matrix effects. A systematic evaluation of matrix effects was done for the matrices previously mentioned: 2% HNO_3, 10% HNO_3, 20% HNO_3, 10% HCl; 500 mg kg^{-1} Na, 500 mg kg^{-1} Na + 10% HNO_3, 10% ethanol, 10% acetic acid and 10% formic acid (percentage in *w*/w). When complex and/or solid samples are analyzed, it is mandatory to apply a previous sample treatment step. One of the most common methodologies is acid digestion of the sample. Depending on the sample nature, different acids and concentrations could be employed, typically not exceeding 20% in the final digested samples. On the other hand, certain environmental samples, such as seawater, or some clinical samples, may have a high content of sodium. In such cases, a common approach is to dilute the sample by at least 10 times to mitigate matrix effect. Additionally, three organic compounds were selected as they could be used for sample preparation. Concentrations higher than 10% were not used because in those cases, due to the volatility of the compounds, sample dilution is usually required. Finally, environmental, clinical and ethanolic matrix samples were analyzed.

3.1. Evaluation of critical variables: Gas flow rate and temperature

The effect of the nebulizer gas flow rate on the ICP-MS/MS signal intensity was evaluated. Fig. S2 (Appendix) shows the results obtained for Cu, Ni, Mn, Pb and V, since comparable observations could be made for other measured analytes. It was observed that most of the elements behaved as Mn and V and the signal intensity peaked at 0.3 L min^{-1}. However, the maximum signal intensity for Cu, Ni and Pb was obtained for a slightly higher nebulizer gas flow rate (*i.e.*, 0.4–0.5 L min^{-1}). Greater values of the nebulization flow rate caused a shortening in the residence time of the sample aerosol inside the IR-TSC, leading to a reduction in solvent pre-evaporation before reaching the plasma. Additionally, high values of nebulization gas flow rate could degrade the plasma thermal characteristics and shorten the residence time of the analyte in the plasma.

When considering the $^{36}Ar^+$ signal intensity (Fig. S3A (Appendix)), it was observed that this parameter remained constant. Due to their comparable atomic masses and distinct first ionization potentials, changes in plasma conditions impact the $^9Be^+/^7Li^+$ ratio, increasing for most robust plasmas [26]. As Fig. S3B (Appendix) shows, modifying the gas flow rate did not result in any modifications to the $^9Be^+/^7Li^+$ ratio. A similar behavior was found for the CeO^+/Ce^+ ratio, expressed as a percentage (Fig. S3C (Appendix)).

In order to evaluate the effect of the temperature of the spray chamber on the analytical signal, the intensity obtained for each temperature was normalized with respect to the signal intensity obtained for the IR-TSC at room temperature (Fig.S4A (Appendix)). The analytical signal rose significantly when the temperature increased from room temperature to 105 °C, this indicated that almost the totality of the nebulized sample was delivered to the plasma at this temperature. In fact, when the temperature was 105 °C or higher, the formation of droplets on the inner surface of the spray chamber was not observed. For most elements, the maximum signal intensity was obtained at 125 °C. At the optimum temperature, the normalized intensity was included within the 2.5 to 5 range, depending on the analyte. Moreover, it was observed

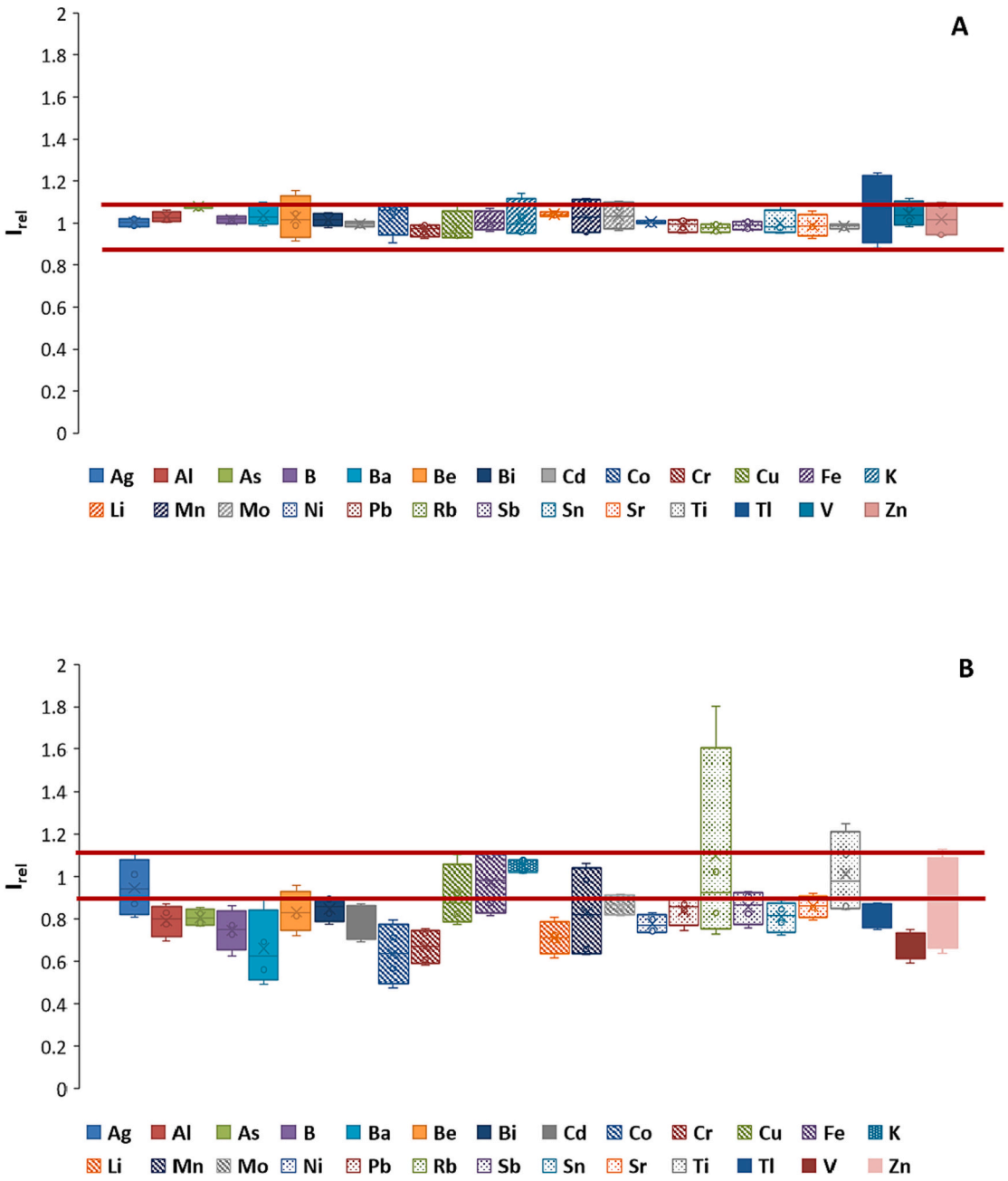

Fig. 2. Relative intensity values (I_{rel}) obtained for the aqueous matrices analyzed with (a) IR-TSC at 125 °C and (b) conventional sample introduction system. Experimental operating conditions described in Table S2 (Appendix). Analyte concentration: 50 μg L^{-1}.

that both excessively low temperatures and temperatures above 125 °C led to a degradation in the signal stability (Fig.S4B (Appendix)). As a result, 125 °C was selected as optimum value.

When considering $^{36}Ar^{+}$ signal intensity (Fig. S5A (Appendix)), it was observed that the signal intensity increased with chamber temperature up to 105 °C. However, $^{36}Ar^{+}$ signal intensity remained constant above this temperature. As Fig. S4B (Appendix) shows, the highest $^{9}Be^{+}/^{7}Li^{+}$ ratio was found at 105 and 125 °C spray chamber temperatures. Both datasets suggested that an increase in the mass of water reaching the plasma enhanced its thermal conductivity, as it has been anticipated by several authors under conditions leading to a robust plasma [27]. Moreover, the CeO^{+}/Ce^{+} ratio, expressed as a percentage, was close to 1.25% at room temperature, whereas at higher temperatures, the IR-TSC provided slightly higher ratios due to an enhancement in the mass of solvent reaching the plasma (Fig. S5C (Appendix)).

3.2. Comparison with a conventional sample introduction system

The results obtained using the infrared-heated total sample consumption system (IR-TSC) were compared with those provided by a conventional sample introduction system. The optimum experimental conditions in terms of signal intensity were used for both sample introduction systems (Table S2 (Appendix)). It is important to note that, for the conventional sample introduction system, a liquid flow rate of 0.8 mL min^{-1} was used for aqueous matrices, while for organic matrices, the liquid flow rate was reduced to 0.1 mL min^{-1} to prevent plasma extinction. Although the liquid flow rate for the IR-TSC was approximately 25 times lower for aqueous matrices and 3 times lower for organic matrices compared to the conventional system, as Fig. 1 shows, the signal intensity obtained with the former device was higher than that measured using the conventional one. This was a clear advantage of the

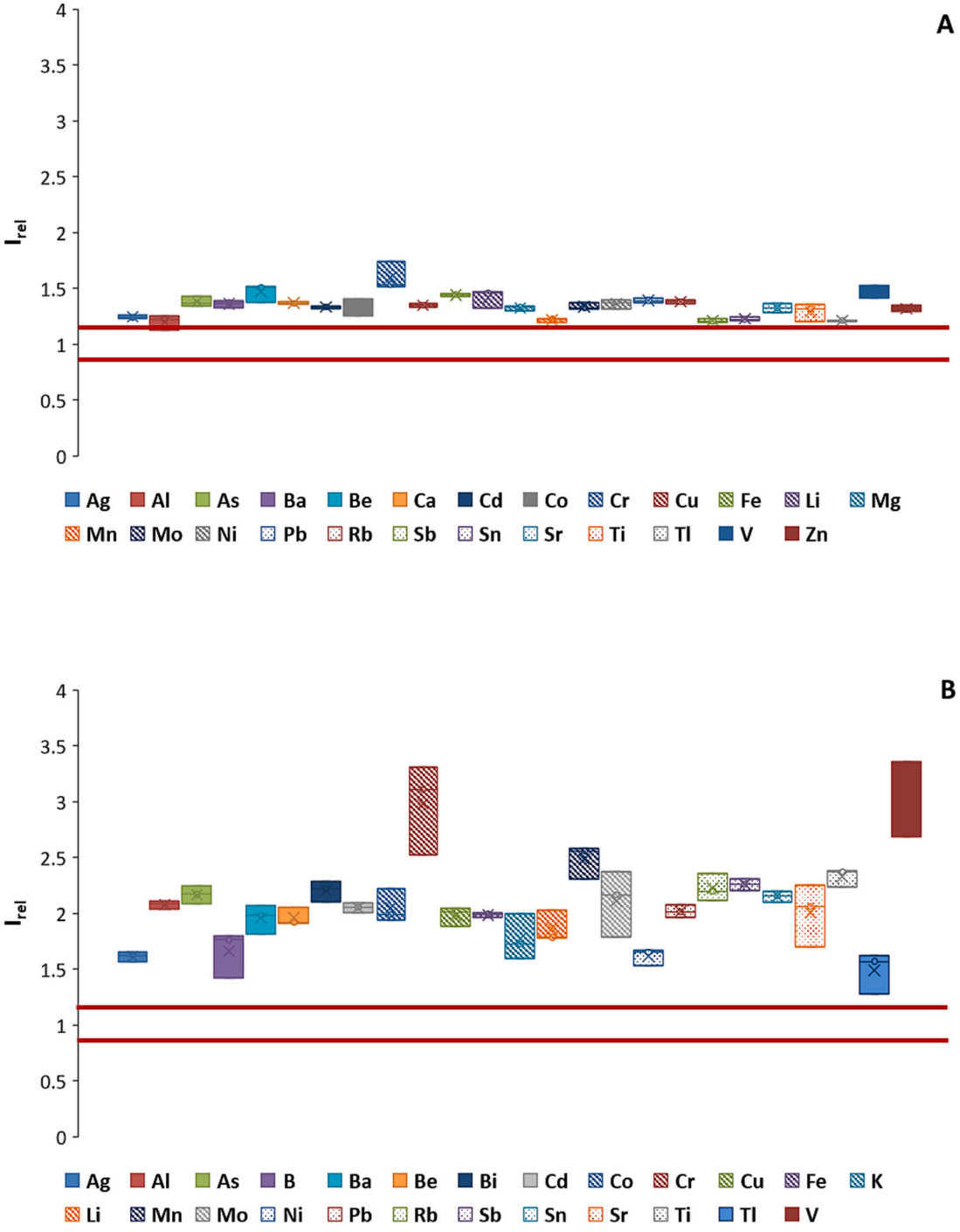

Fig. 3. Relative values (I_{rel}) obtained for the organic matrices analyzed with (a) IR-TSC at 125 °C and (b) conventional sample introduction system. No internal standard has been used. Experimental operating conditions described in Table S2 (Appendix). Analyte concentration: 50 μg L^{-1}.

increased analyte transport efficiency induced by the work at high chamber temperatures [20]. For aqueous matrices, IR-TSC provided signal intensities that were from 2 to 4 times higher than those for the conventional setup for all elements. However, the improvement factor for organic matrices was below 2. Limits of detection (LOD) were calculated according to the $3s_b$ criterion, where s_b was the standard deviation of ten independent blank replicates. For all the elements evaluated, higher LODs were obtained for the conventional sample introduction system than for the IR-TSC (Table 1). The improvement factor ranged from 1.2 (Ba) to 3.3 (Cr) for 2% HNO_3 matrices, while for ethanol matrices the improvement factor ranged from 1.4 (Ti) to 3.8 (Cr).

3.3. Matrix effects

Matrix effects were studied under optimal sensitivity conditions for two sets of matrices. Six inorganic (2% HNO_3, 10% HNO_3, 20% HNO_3, 20% HCl, 500 mg L^{-1} Na, and, 500 mg L^{-1} Na + 10% HNO_3) and three organic matrices (10% ethanol, 10% acetic acid, and, 10% formic acid) were studied. The net signal intensity obtained for each sample was normalized with respect to the net signal intensity obtained for the 2% HNO_3 matrix. Therefore, a relative value (I_{rel}) equal to unity meant that

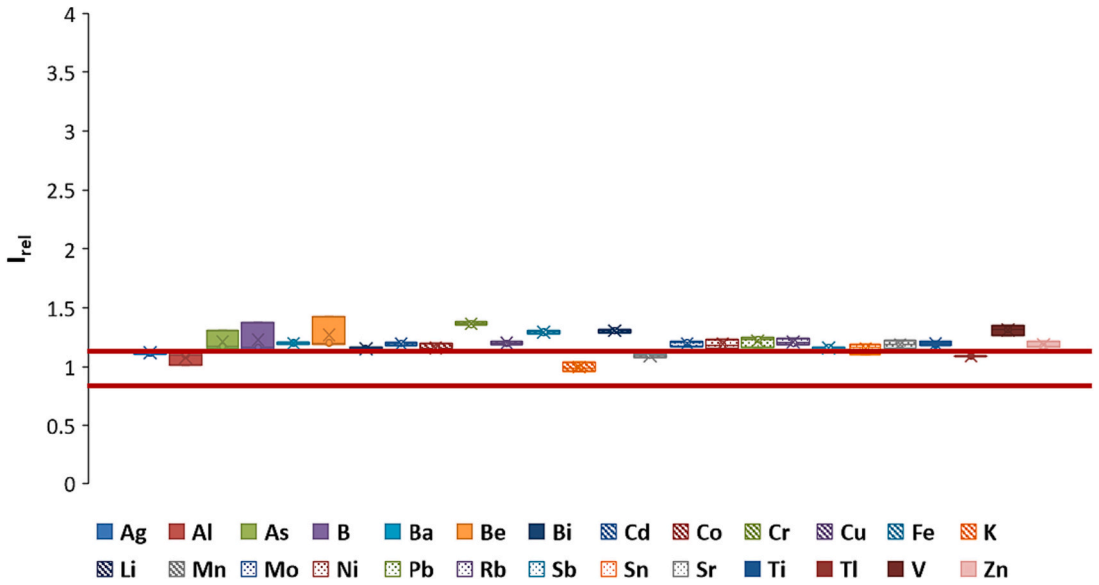

Fig. 4. Relative values (I_{rel}) obtained for the organic matrices analyzed with IR-TSC at 125 °C sample introduction system. Internal standard has been used. Experimental operating conditions described in Table S2 (Appendix). Analyte concentration: 50 μg L^{-1}.

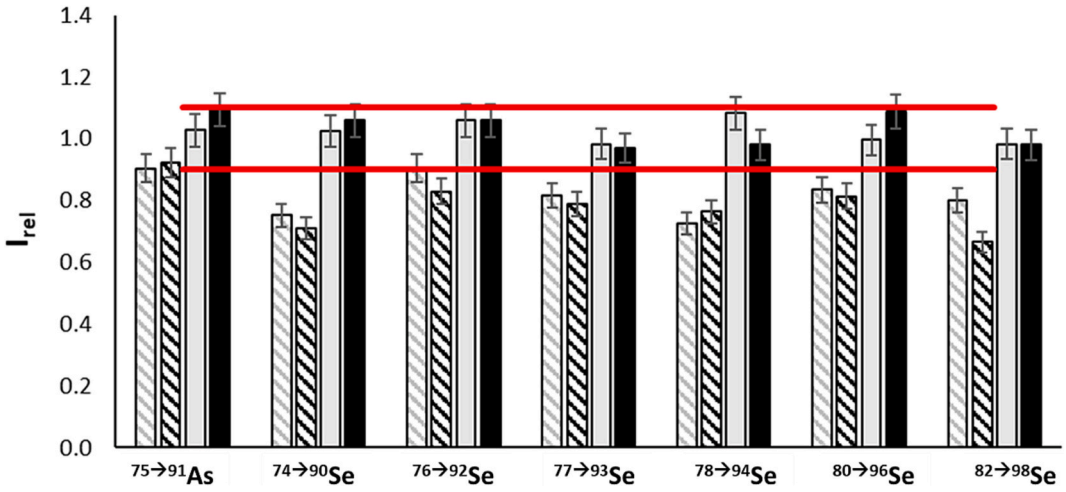

Fig. 5. Relative intensity values (I_{rel}) obtained for 10% HNO_3 (grey) and 10% HCl (black) matrices analyzed with IR-TSC at 125 °C (full bars) and conventional (striped bars) sample introduction system. Experimental operating conditions described in Table S2 (Appendix). Analyte concentration: 50 μg L^{-1}.

matrix effects were minimized. Fig. 2 and Fig. 3 show the I_{rel} obtained for the IR-TSC and for the conventional sample introduction system. Additionally, Fig. S6, S7, S8, S9, S10, S11, S12 and S13 (Appendix) show the matrix effect for each specific sample analyzed.

It is well known that the presence of acids and easily ionizable elements could cause matrix effects, thus affecting the accuracy of the results [5,9,28]. When the IR-TSC was used, the median relative values were close to unity (Fig. 2A). In contrast, when the conventional sample introduction system was used, significant matrix effects were observed (Fig. 2B). The median value for most of the elements ranged from 0.70 to 0.85. Moreover, the dispersion of the data was more significant for the conventional sample introduction system than for the IR-TSC.

However, when analyzing samples containing organic solvents, significant matrix effects were observed for both sample introduction systems (Fig. 3). Although the median relative intensity for the IR-TSC was closer to unity compared to the conventional system, a matrix effect was still present. The signal intensity for the solutions containing organic solvents was around 50% higher than for 2% HNO_3 matrix, taken as reference (Fig. 3, Fig. S11, Fig. S12 and Fig. S13 (Appendix)). This behavior could be explained by changes in the absorbed IR energy of the different compounds evaluated as matrices. Fig. S14 shows the absorption spectrum for the emission wavenumber range of the IR lamps used in the IR-TSC device. Significant differences could be observed in the spectra for the pure compounds (*i.e.*, water, ethanol, acetic acid, and formic acid). Although water was the major component of the sample matrix, the presence of organic compounds could lead to differences in IR absorption compared to the reference solution (2% HNO_3). As a result, the heating efficiency depended on the matrix, thus, affecting the improvement of the analyte transport efficiency towards the plasma and leading to relative intensity values higher than unity (Fig. 3A). In addition, no differences were observed in the thermal characteristics and robustness of the plasma (Fig. S15 (Appendix)). This confirmed that the source of matrix effects was the change in analyte transport efficiency towards the plasma. One possible approach to mitigate this situation is the use of an internal standard. However, as shown in Fig. 4, Fig. S16, Fig. S17 and Fig. S18 (Appendix), this solution did not completely remove matrix effects for all the evaluated elements. The relative intensity values found were in the range of 1.00 to 1.30. Indeed,

Table 2
Analyte concentration (μg L^{-1}) certified and measured for each certified reference samples obtained by the IR-TSC at 125 °C coupled to an ICP-MS/MS. n.c.: value not certified; #: reference value; *: out of the calibration range; @: $^{78\rightarrow94}$Se.

Sample	Ag		Al		As		Ba		Bi		Cd		Co	
	IR-TSC	*Certified value*	*IR-TSC*	*Certified value*	*IR-TSC*	*Certified value*	*IR-TSC*	*Certified value*	*IR-TSC*	*Certified value*	*IR-TSC*	*Certified value*	*IR-TSC*	*Certified value*
Clinchek Urine II	**5.6 ± 0.5**	**5.3 ± 1.3**	**86 ± 6**	**82 ± 16**	**77 ± 5**	**82 ± 16**	**50 ± 3**	**50 ± 10**	< 0.3	**15 ± 3**	**14.2 ± 1.4**	**15 ± 3**	**10.8 ± 1.0**	**10 ± 2**
Seronorm	< 0.2	n.c.	**102 ± 6**	**100 ± 20**	**27 ± 4**	**30 ± 7**	**690 ± 60**	**700 ± 15**	**56 ± 5**	**12.1 ± 1.3**	**12.5 ± 1.3**	**12.1 ± 1.3**	**10.2 ± 0.9**	**11.4 ± 1.2**
CASS 6	< 0.2	n.c.	< 0.2	n.c.	**0.97 ± 0.12**	**1.04 ± 0.10#**	< 0.3	n.c.	< 0.3	0.0213 ± 0.0018	< 0.13	0.0213 ± 0.0018	< 0.4	0.066 ± 0.005
NASS 5	< 0.2	n.c.	< 0.2	n.c.	1.44 ± 0.05	1.27 ± 0.12	< 0.3	n.c.	< 0.3	0.023 ± 0.003	< 0.13	0.023 ± 0.003	< 0.4	0.011 ± 0.003
ERM CA 403	< 0.2	n.c.	< 0.2	n.c.	**1.95 ± 0.12**	**1.90 ± 0.13**	< 0.3	n.c.	< 0.3	0.094 ± 0.011	< 0.13	0.094 ± 0.011	< 0.4	0.074 ± 0.011
Sample	**Cr**		**Cu**		**Fe**		**Li**		**Mn**		**Ni**		**Pb**	
	IR-TSC	*Certified value*	*IR-TSC*	*Certified value*	*IR-TSC*	*Certified value*	*IR-TSC*	*Certified value*	*IR-TSC*	*Certified value*	*IR-TSC*	*Certified value*	*IR-TSC*	*Certified value*
Clinchek Urine II	**9.3 ± 0.5**	**10 ± 2**	**106 ± 7**	**115 ± 23**	**216 ± 15**	**222 ± 45**	< 0.3	n.c.	**10.8 ± 1.0**	**10 ± 2**	**15.4 ± 1.0**	**15 ± 3**	**47 ± 6**	**52 ± 10**
Seronorm	**24.3 ± 0.7**	**23 ± 5**	**2300 ± 300**	**2500 ± 200**	250,000 ± 30000*	380,000 ± 10,000	0.43 ± 0.04	0.36 ± 0.03	**45 ± 2**	**47 ± 10**	**13.2 ± 1.1**	**13 ± 3**	**420 ± 30**	**450 ± 50**
CASS 6	3.86 ± 0.11	0.098 ± 0.016	0.76 ± 0.11	0.52 ± 0.03	< 1.8	1.53 ± 0.12	< 0.3	n.c.	1.90 ± 0.05	2.18 ± 0.12	**0.41 ± 0.02**	**0.410 ± 0.040**	< 0.09	0.0104 ± 0.0040
NASS 5	< 0.5	0.110 ± 0.015	< 0.4	0.30 ± 0.05	< 1.8	0.28 ± 0.04	< 0.3	n.c.	**0.95 ± 0.07**	**0.92 ± 0.06**	< 0.4	0.263 ± 0.028	< 0.09	0.008 ± 0.005
ERM CA 403	< 0.5	n.c.	**0.81 ± 0.09**	**0.87 ± 0.13**	3.1 ± 0.4	n.c.	< 0.3	n.c.	**2.4 ± 0.2**	**2.47 ± 0.11**	**0.83 ± 0.14**	**1.04 ± 0.16**	< 0.09	0.098 ± 0.010
Sample	**Se@**		**Sr**		**Ti**		**Tl**		**V**		**Zn**			
	IR-TSC	*Certified value*	*IR-TSC*	*Certified value*	*IR-TSC*	*Certified value*	*IR-TSC*	*Certified value*	*IR-TSC*	*Certified value*	*IR-TSC*	*Certified value*		
Clinchek Urine II	**72 ± 8**	**79 ± 16**	1.40 ± 0.15	n.c.	890 ± 40	n.c.	**20 ± 2**	**19 ± 4**	**55 ± 3**	**52 ± 10**	**585 ± 60**	**600 ± 120**		
Seronorm	**289 ± 19**	**272 ± 55**	**13.2 ± 1.2**	**15.0 ± 0.2**	11.3 ± 0.6	12.8 ± 0.4	**35 ± 10**	**34 ± 7**	**5.3 ± 0.3**	**5.7 ± 1.1**	**8500 ± 1000***	**9000 ± 700**		
CASS 6	< 2.5	n.c.	< 0.14	n.c.	3.6 ± 0.2	n.c.	< 0.11	n.c.	**0.55 ± 0.05**	**0.49 ± 0.12**	**1.31 ± 0.14**	**1.24 ± 0.18**		
NASS 5	< 2.5	n.c.	< 0.14	n.c.	< 0.4	n.c.	< 0.11	n.c.	0.96 ± 0.09	1.2	< 0.3	0.10 ± 0.04		
ERM CA 403	< 2.5	n.c.	< 0.14	n.c.	< 0.4	n.c.	< 0.11	n.c.	< 0.12	n.c.	**5.6 ± 0.6**	**4.6 ± 0.6**		

the observed matrix effects appear to be influenced not only by the analyte transport efficiency but also by the spatial distribution of the ion cloud in the plasma. The presence of organic solvents resulted in ions being generated in close proximity to the coil, leading to a greater likelihood of ionic plasma radial diffusion. As a result, the spatial distribution of ions within the plasma became dependent on the composition of the sample matrix [29].

3.4. Analytes spectrally interfered

Once the capability of the IR-TSC at 125 °C to minimize matrix effects was demostrated, the addition of oxygen as collision/reaction gas was explored. Some challenging analytes, such as As and Se, suffering from polyatomic interferences, were determined. Analyte signal intensities were obtained for a 50 μg L^{-1} multielemental solution, for three different matrices: 2% HNO_3, 10% HNO_3 and 10% HCl. As for non-spectrally interfered analytes, the signal intensity obtained with the IR-TSC at 125 °C was higher than that measured using the conventional sample introduction system (Fig. S19 (Appendix)). Additionally, a relative value (I_{rel}) equal to unity was found for the IR-TSC at 125 °C (Fig. 5), meaning that matrix effects were again minimized for the two matrices evaluated, 10% HNO_3 and 10% HCl, taking as reference 2% HNO_3.

Regarding LOD, lower values were found for the IR-TSC sample introduction system (Table S3 (Appendix)). It is worth noting that the detection limits found for As in He mode (Table 1) were lower than those found when oxygen was used as the reaction/collision gas. Therefore, since accurate results were obtained with the former working mode, He mode was employed for the analysis of the samples.

3.5. Analysis of samples

The results obtained so far indicated that the IR-TSC at 125 °C yielded a minimization of matrix effects for inorganic matrices, such as acids and high content of sodium. In order to validate this hypothesis, the certified and control samples listed in Table S1 (Appendix) were analyzed. A dilution factor equal to 10 was applied to all the certified and control samples. For external calibration, without the use of internal standard, the concentration range for the standards was from 0.05 to 250 μg L^{-1}. Table 2 shows the concentration and certified values for the analyzed samples. To simplify the table, only the results for those elements with certified concentration have been included. In addition, the

Table 3
Analyte concentration (μg L^{-1}) for aqueous samples obtained by the IR-TSC at 125 °C coupled to an ICP-MS/MS. *: out of the calibration range.

Sample	B	Ba	Be	Bi	Cd	Co	Cr	Cu	Fe	Li	Mn
Seawater (1)	< 0.4	< 0.3	< 0.3	< 0.3	< 0.13	< 0.4	0.56 ± 0.04	< 0.4	< 1.8	< 0.3	3.3 ± 0.2
Seawater (2)	< 0.4	< 0.3	< 0.3	< 0.3	< 0.13	< 0.4	< 0.5	< 0.4	< 1.8	< 0.3	2.57 ± 0.11
Continental surface water (1)	< 0.4	< 0.3	< 0.3	0.33 ± 0.07	< 0.13	< 0.4	< 0.5	0.87 ± 0.10	2.18 ± 0.15	< 0.3	4.1 ± 0.3
Continental surface water (2)	< 0.4	< 0.3	< 0.3	< 0.3	< 0.13	< 0.4	0.72 ± 0.08	0.62 ± 0.05	< 1.8	0.34 ± 0.07	3.83 ± 0.09
Peritoneal fluid (1)	< 0.4	8.6 ± 0.4	< 0.3	1.71 ± 0.14	0.372 ± 0.008	3.1 ± 0.2	11.2 ± 0.9	879 ± 5	3490 ± 30*	1.91 ± 0.12	5.78 ± 0.11
Peritoneal fluid (2)	0.49 ± 0.05	23.7 ± 1.0	< 0.3	6.91 ± 0.08	2.65 ± 0.04	1.038 ± 0.009	12.3 ± 1.1	1098 ± 8	2565 ± 19*	4.02 ± 0.14	14.5 ± 0.3
Plasma seminal (1)	< 0.4	< 0.3	0.52 ± 0.04	< 0.3	< 0.13	1.23 ± 0.07	83 ± 2	61.7 ± 1.8	470 ± 20	< 0.3	8.72 ± 0.11
Plasma seminal (2)	< 0.4	1.23 ± 0.03	0.371 ± 0.008	< 0.3	< 0.13	< 0.4	92 ± 3	87 ± 4	540 ± 30	< 0.3	12.8 ± 0.4
Sample	**Mo**	**Ni**	**Pb**	**Rb**	**Sb**	**Sn**	**Sr**	**Ti**	**Tl**	**V**	**Zn**
Seawater (1)	< 0.3	< 0.4	< 0.09	< 0.3	< 0.3	0.223 ± 0.008	< 0.14	< 0.4	< 0.11	0.94 ± 0.06	1.47 ± 0.12
Seawater (2)	< 0.3	< 0.4	< 0.09	< 0.3	< 0.3	< 0.10	< 0.14	< 0.4	< 0.11	1.14 ± 0.07	1.73 ± 0.14
Continental surface water (1)	< 0.3	0.45 ± 0.06	< 0.09	< 0.3	0.34 ± 0.04	< 0.10	0.31 ± 0.04	< 0.4	< 0.11	1.61 ± 0.13	6.4 ± 0.3
Continental surface water (2)	< 0.3	0.52 ± 0.06	< 0.09	< 0.3	< 0.3	< 0.10	0.204 ± 0.006	< 0.4	0.153 ± 0.008	2.03 ± 0.09	4.1 ± 0.3
Peritoneal fluid (1)	0.42 ± 0.03	3.6 ± 0.2	< 0.09	67 ± 5	< 0.3	3.7 ± 0.3	11.1 ± 0.6	29.3 ± 1.7	< 0.11	55.8 ± 1.8	3370 ± 30*
Peritoneal fluid (2)	< 0.3	9.8 ± 0.4	2.3 ± 0.2	38 ± 3	< 0.3	5.2 ± 0.3	34 ± 2	72 ± 3	0.19 ± 0.02	38 ± 2	9120 ± 120*
Plasma seminal (1)	6.13 ± 0.06	< 0.4	< 0.09	< 0.3	< 0.3	0.703 ± 0.018	83 ± 7	47 ± 2	< 0.11	8.7 ± 0.6	427 ± 18
Plasma seminal (2)	4.96 ± 0.37	0.69 ± 0.05	< 0.09	< 0.3	< 0.3	0.47 ± 0.03	77 ± 4	33.6 ± 1.8	< 0.11	14.2 ± 0.9	750 ± 20

procedural limit of quantification (pLOQ) was calculated by taking into account the limit of quantification and the dilution factor (Table S4 (Appendix)).

The results were evaluated by comparing the difference (Δ_m) between certified and measured values with the combined uncertainty (U_Δ) of the certified and measured values. Eq. 2 was applied to calculate the absolute difference between the mean measured value and the certified value. The uncertainty u_Δ was obtained from the uncertainty of the certified value and the standard deviation of the measurement result (Eq. 3), and the expanded uncertainty U_Δ was obtained by multiplying u_Δ by a coverage factor (k), usually equal to 2, corresponding to a confidence level of approximately 95%. The method performance was evaluated by comparing Δ_m with U_Δ [30]. As Δ_m was lower than U_Δ for the majority of the elements, it was concluded that there were no statistically significant differences between values obtained experimentally and the certified concentrations (Table S5 (Appendix)).

$$\Delta_m = |c_m - c_{CRM}| \tag{2}$$

$$u_\Delta = \sqrt{s_m^2 + u_{CRM}^2} \tag{3}$$

where c_m is the mean measured value, c_{CRM} is the certified value, s_m is the standard deviation of the measurement, and u_{CRM} is the uncertainty of the certified value.

Based on the above discussed results, aqueous real samples were analyzed, as an example of the application fields (Table 3 and Table S6 (Appendix)). A dilution factor of 10 was applied to all samples. Additionally, to evaluate the potential of the IR-TSC method for routine analysis, an internal standard calibration strategy was used. As an example of application to environmental sample analysis, two seawaters and two continental surface waters were analyzed. The Water Framework Directive (WFD) [31] includes a list of priority substances that present a risk for the good chemical status of the aquatic ecosystems defined in terms of compliance with all the environmental quality standards (EQSs) laid out in the daughter Directive 2013/39/EU [32]. As inorganic contaminants, the list includes cadmium, nickel, and lead. The EQS expressed as a maximum allowable concentration (MAC) is 0.45, 34 and 14 μg L^{-1}, respectively. As Table 3 shows, the determined concentration of these metals in the real water samples was below the established legal limit.

Besides, as an example of application to clinical sample analysis, peritoneal fluid and seminal plasma samples have been analyzed. Although some metals such as manganese can be considered essential, the presence of others may be closely related to problems in human reproduction [33,34]. For example, a high Cd and Pb exposition increases its concentration in semen, causing lower sperm motility or affecting the estrogenic activity [35–38].

Although matrix effects were not completely eliminated in the case of the solutions containing organic solvents, two samples with ethanol in their composition were included among the analyzed samples (Table S6 (Appendix)). In the wine sample, elements related to external practices (Fe, Mn and Zn) were present at relatively high concentration (> 500 μg L^{-1}). The content of other elements, such as Cr, Cu, Mo, Ni, Pb, Ti and V ranged from 20 to 120 μg L^{-1} [39–43]. Meanwhile, metal contamination could occur in bioethanol samples during production, storage, and transport. For bioethanol samples previous works reported that some trace elements, such as Cu, Fe, Mn, Ni or Zn, were found at concentrations ranging from 1 to 100 ng mL^{-1} [44–46], however Mn, Ni and Zn were present in the samples analyzed at higher concentration (Table S6 (Appendix)).

The results obtained by using IR-TSC were compared with previously published and validated results obtained for the same samples [43,47]. Concentration values were statistically compared. When variances could be considered statistically comparable, the concentrations obtained were evaluated by means of the t-Student test. If the variances were not statistically comparable, t-value and the degree of freedom were calculated by applying the following equations:

$$t = \frac{(\overline{x}_1 - \overline{x}_2)}{\sqrt{\frac{s_1^2}{n_1} + \frac{s_2^2}{n_2}}} \quad (4)$$

$$Degrees\ of\ freedom = \frac{\left(\frac{s_1^2}{n_1} + \frac{s_2^2}{n_2}\right)^2}{\left(\frac{s_1^4}{n_1^2(n_1-1)} + \frac{s_2^4}{n_2^2(n_2-1)}\right)} \quad (5)$$

where $\overline{x}$ was the mean value, s was the standard deviation and n was the number of replicates of method 1 or 2. As it was expected from the recovery results (Section 3.3), the accuracy was poor for the analysis of sample solutions containing organic solvents. Therefore, the concentrations obtained using the IR-TSC sample introduction system differed from the validated values [44,47]. Statistically comparable results were provided by both methods only in 11 out of the 52 evaluated cases (Table S6, Table S7 and Table S8 (Appendix)).

4. Conclusions

This study introduces the adaptation of the infrared-heated total sample consumption system (IR-TSC) to ICP-MS/MS, which demonstrated an improvement of the analytical performance for the analysis of inorganic acid samples and solutions containing high concentrations of sodium. Under optimized experimental conditions, the IR-TSC at 125 °C showed several advantages over the conventional setup: (i) higher sensitivity; (ii) lower limits of detection; and (iii) mitigation of matrix effects for aqueous samples. As a result, accurate analysis of environmental and clinical certified reference samples could be carried out using external calibration. Consequently, IR-TSC may expand the field of application of ICP-MS/MS for the elemental analysis of solutions containing inorganic acids and high salt content. Moreover, the combination of the IR-TSC at 125 °C with the ICP-MS/MS configuration removed spectral as well as non-spectral interferences, thus allowing the accurate determination of analytes such as As and Se.

Regarding samples containing organic solvents, although the infrared-heated total sample consumption system (IR-TSC) could reduce matrix effects, complete elimination has not yet been achieved. Further efforts will involve modifying the IR-TSC chamber geometry, IR source and experimental conditions to try to fully eliminate organic matrix effects.

CRediT authorship contribution statement

Raquel Sánchez: Conceptualization, Data curation, Formal analysis, Investigation, Methodology, Resources, Supervision, Validation, Visualization, Writing – original draft, Writing – review & editing. **José-Luis Todolí:** Conceptualization, Funding acquisition, Investigation, Methodology, Project administration, Resources, Supervision, Validation, Visualization, Writing – original draft, Writing – review & editing.

Declaration of competing interest

The authors declare that they have no known competing financial interests or personal relationships that could have appeared to influence the work reported in this paper.

Data availability

Data will be made available on request.

Acknowledgments

The authors wish to thank the Spanish Ministry of Science, Innovation, and Universities for the financial support (Projects Ref. PGC2018-100711-B-I00 and PID2021-127566NB-I00).

Appendix A. Supplementary data

Supplementary data to this article can be found online at https://doi.org/10.1016/j.sab.2023.106779.

References

[1] A. Montaser, Inductively Coupled Plasma Mass Spectrometry, Wiley-VCH, Weinheim, 1998.
[2] E.H. Evans, J.J. Giglio, Interferences in inductively coupled plasma mass spectrometry. A review, J. Anal. At. Spectrom. 8 (1993) 1–18, https://doi.org/10.1039/JA9930800001.
[3] R.F.J. Dams, J. Goossens, L. Moens, Spectral and non-spectral interferences in inductively coupled plasma mass-spectrometry, Mikrochim. Acta 119 (1995) 277–286, https://doi.org/10.1007/BF01244007.
[4] T.W. May, R.H. Wiedmeyer, A table of polyatomic interferences in ICP-MS, At. Spectrosc. 19 (1998) 150–155, https://doi.org/10.46770/AS.1998.05.002.
[5] C. Agatemor, D. Beauchemin, Matrix effects in inductively coupled plasma mass spectrometry: a review, Anal. Chim. Acta 706 (2011) 66–83, https://doi.org/10.1016/j.aca.2011.08.027.
[6] T.S. Luma, K.S.Y. Leung, Strategies to overcome spectral interference in ICP-MS detection, J. Anal. At. Spectrom. 31 (2016) 1078–1088, https://doi.org/10.1039/C5JA00497G.
[7] L. Balcaen, E. Bolea-Fernandez, M. Resano, F. Vanhaecke, Inductively coupled plasma - tandem mass spectrometry (ICP-MS/MS): a powerful and universal tool for the interference-free determination of (ultra)trace elements – a tutorial review, Anal. Chim. Acta 894 (2015) 7–19, https://doi.org/10.1016/j.aca.2015.08.053.
[8] E. Bolea-Fernandez, L. Balcaen, M. Resano, F. Vanhaecke, Overcoming spectral overlap via inductively coupled plasma-tandem mass spectrometry (ICP-MS/MS). A tutorial review, J. Anal. At. Spectrom. 32 (2017) 1660–1679, https://doi.org/10.1039/C7JA00010C.
[9] M. Grotti, J.L. Todolí, Nitric acid effect in inductively coupled plasma mass spectrometry: new insights on possible causes and correction, J. Anal. At. Spectrom. 35 (2020) 1959–1968, https://doi.org/10.1039/D0JA00130A.
[10] J.L. Todolí, J.M. Mermet, Acid interferences in atomic spectrometry: analyte signal effects and subsequent reduction, Spectrochim. Acta, Part B 54 (1999) 895–929, https://doi.org/10.1016/S0584-8547(99)00041-5.
[11] J.L. Todolí, J.M. Mermet, Minimization of acid effects at low consumption rates in an axially viewed inductively coupled plasma atomic emission spectrometer by using micronebulizer-based sample introduction systems, J. Anal. At. Spectrom. 13 (1998) 727–734, https://doi.org/10.1039/A801124I.
[12] J.W. Olesik, S. Jiao, Matrix effects using an ICP-MS with a single positive ion lens and grounded stop: analyte mass dependent? J. Anal. At. Spectrom. 32 (2017) 951–966, https://doi.org/10.1039/C7JA00043J.
[13] K. Kahen, B.W. Acon, A. Montaser, Modified Nukiyama–Tanasawa and Rizk–Lefebvre models to predict droplet size for microconcentric nebulizers with aqueous and organic solvents, J. Anal. At. Spectrom. 20 (2005) 631–637, https://doi.org/10.1039/B501186H.
[14] M.S. Cresser, R.F. Browner, A method for investigating size distributions of aqueous droplets in the range 0.5–10 μm produced by pneumatic nebulizers, Spectrochim. Acta, Part B 35 (1980) 73–79, https://doi.org/10.1016/0584-8547(80)80054-1.
[15] B.L. Sharp, Pneumatic nebulisers and spray chambers for inductively coupled plasma spectrometry. A review. Part 2. Spray chambers, J. Anal. At. Spectrom. 3 (1988) 939–963, https://doi.org/10.1039/JA9880300939.
[16] A. Leclercq, A. Nonell, J.L. Todolí, C. Bresson, L. Vio, T. Vercouter, F. Chartier, Introduction of organic/hydro-organic matrices in inductively coupled plasma optical emission spectrometry and mass spectrometry: a tutorial review. Part I. theoretical considerations, Anal. Chim. Acta 885 (2015) 33–56, https://doi.org/10.1016/j.aca.2015.03.049.
[17] J.M. Mermet, Revisitation of the matrix effects in inductively coupled plasma atomic emission spectrometry: the key role of the spray chamber, J. Anal. At. Spectrom. 13 (1998) 419–422, https://doi.org/10.1039/A707197C.
[18] Y. Makonnen, J. Burgener, D. Beauchemin, Improvement of analytical performance in inductively coupled plasma optical emission spectrometry without compromising robustness using an infrared-heated sample introduction system with a pneumatic nebulizer, J. Anal. At. Spectrom. 30 (2015) 214–224, https://doi.org/10.1039/C4JA00258J.
[19] A. Al Hejami, D. Beauchemin, Infrared heating of commercially available spray chambers to improve the analytical performance of inductively coupled plasma optical emission spectrometry, J. Anal. At. Spectrom. 33 (2018) 2008–2014, https://doi.org/10.1039/C8JA00239H.
[20] A. Al Hejami, D. Beauchemin, Infrared heating of the top surface of a cyclonic spray chamber to improve the analytical performance of inductively coupled plasma optical emission spectrometry, J. Anal. At. Spectrom. 34 (2019) 232–238, https://doi.org/10.1039/C8JA00363G.
[21] A. Al Hejami, D. Beauchemin, New infrared-heated sample introduction system for enhanced analytical performance of inductively coupled plasma optical emission spectrometry, J. Anal. At. Spectrom. 33 (2018) 738–744, https://doi.org/10.1039/C8JA00044A.
[22] A. Al Hejami, M.J. Burgener, J. Burgener, D. Beauchemin, A total consumption (up to 75 μL min−1) infrared-heated sample introduction system for inductively coupled plasma optical emission spectrometry, J. Anal. At. Spectrom. 35 (2020) 1125–1130, https://doi.org/10.1039/D0JA00068J.

[23] R. Teuma-Castelletti, A. Al Hejami, D. Beauchemin, An infrared-heated sample introduction system for inductively coupled plasma mass spectrometry, At. Spectrosc. 43 (2022) 371–377, https://doi.org/10.46770/AS.2022.233.
[24] Z. Zhou, A. Al Hejami, M.J. Burgener, J. Burgener, D. Beauchemin, A total consumption infrared heated sample introduction system for nanoparticle measurement using single particle inductively coupled plasma mass spectrometry, J. Anal. At. Spectrom. 37 (2022) 1450–1454, https://doi.org/10.1039/D2JA00059H.
[25] M. Grotti, F. Ardini, J.L. Todolí, Total introduction of microsamples in inductively coupled plasma mass spectrometry by high-temperature evaporation chamber with a sheathing gas stream, Anal. Chim. Acta 767 (2013) 14–20, https://doi.org/10.1016/j.aca.2013.01.017.
[26] Y. Makonnen, D. Beauchemin, Investigation of a measure of robustness in inductively coupled plasma mass spectrometry, Spectrochim. Acta Part B 103-104 (2015) 57–62, https://doi.org/10.1016/j.sab.2014.11.010.
[27] I. Novotny, J.C. Farinas, Wan Jia-Liang, E. Poussel, J.M. Mermet, Effect of power and carrier gas flow rate on the tolerance to water loading in inductively coupled plasma atomic emission spectrometry, Spectrochim- Acta Part B 51 (1996) 1517–1526, https://doi.org/10.1016/0584-8547(96)01522-4.
[28] J.L. Todolí, J.M. Mermet, Effect of the spray chamber design on steady and transient acid interferences in inductively coupled plasma atomic emission spectrometry, J. Anal. At. Spectrom. 15 (2000) 863–867, https://doi.org/10.1039/B000589O.
[29] C. Sánchez, R. Sánchez, C.P. Lienemann, J.L. Todolí, ICP-MS spatial profiles in presence of ethanol and their application for the analysis of ethanol containing samples, J. Anal. At. Spectrom. 36 (2021) 2085–2096, https://doi.org/10.1039/D1JA00134E.
[30] T. Linsinger, Application Note 1 Comparison of a Measurement Result with the Certified value, European Commission - Joint Research Centre Institute for Reference Materials and Measurements (IRMM), 2010.
[31] European Commission, Directive 2000/60/EC of the European Parliament and of the council of 23 October 2000 establishing a framework for community action in the field of water policy, Off J Eur Comm L 327 (2000) 1.
[32] European Commission, Directive 2013/39/EU of the European Parliament and of the council of 12 august 2013 on amendment directives 2000/60/EC and 2008/105/EC as regards priority substances in the field of water policy, Off. J. Eur. Union L226 (2013) 1.
[33] K.S. Hruska, P.A. Furth, D.B. Seifer, F.I. Sharara, J.A. Flaws, Environmental factors in infertility, Clin. Obstet. Gynecol. 43 (2000) 821–829, https://doi.org/10.1097/00003081-200012000-00014.
[34] A. López-Botella, I. Velasco, M. Acién, P. Sáez-Espinosa, J.L. Todolí-Torró, R. Sánchez-Romero, M.J. Gómez-Torres, Impact of heavy metals on human male fertility—an overview, Antioxidants 10 (2021) 1473, https://doi.org/10.3390/antiox10091473.
[35] Y. Li, J. Wu, W. Zhou, E. Gao, Association between environmental exposure to cadmium and human semen quality, Int. J. Environ. Health Res. 26 (2015) 175–186, https://doi.org/10.1080/09603123.2015.1061115.
[36] T.K. Jensen, J.P. Bonde, M. Joffe, The influence of occupational exposure on male reproductive function, Occup. Med. 56 (2006) 544–553, https://doi.org/10.1093/occmed/kql116.
[37] P. Rzymski, K. Tomczyk, B. Poniedziałek, T. Opala, M. Wilczak, Impact of heavy metals on the female reproductive system, Ann Agric Environ Med. 22 (2015) 259–264, https://doi.org/10.5604/12321966.1152077.
[38] A. Stoica, B.S. Katzenellenbogen, M.B. Martin, Activation of estrogen receptor-α by the heavy metal cadmium, Mol. Endocrinol. 14 (2000) 545–553, https://doi.org/10.1210/mend.14.4.0441.
[39] J.G. Ibáñez, A. Carreón, A. Lvarez, M. Barcena-Soto, N. Casillas, Metals in alcoholic beverages: a review of sources, effects, concentrations, removal, speciation, and analysis, J. Food Compos. Anal. 21 (2008) 672–683, https://doi.org/10.1016/j.jfca.2008.06.005.
[40] P. Pohl, What do metals tell us about wine? Trends Anal. Chem. 26 (2007) 941–949, https://doi.org/10.1016/j.trac.2007.07.005.
[41] S.M. Rodrigues, M. Otero, A.A. Alves, J. Coimbra, M.A. Coimbra, E. Pereira, A. C. Duarte, Elemental analysis for categorization of wines and authentication of their certified brand of origin, J. Food Compos. Anal. 24 (2011) 548–562, https://doi.org/10.1016/j.jfca.2010.12.003.
[42] B. Tariba, Metals in wine–impact on wine quality and health outcomes, Biol. Trace Elem. Res. 144 (2011) 143–156, https://doi.org/10.1007/s12011-011-9052-7.
[43] C. Cerutti, C. Sánchez, R. Sánchez, F. Ardini, M. Grotti, J.L. Todolí, Determination of trace elements in undiluted wine samples using an automatized total sample consumption system coupled to ICP-MS, J. Anal. At. Spectrom. 34 (2019) 674–682, https://doi.org/10.1039/C8JA00391B.
[44] C. Sánchez, C.P. Lienemann, J.L. Todolí, Analysis of bioethanol samples through inductively coupled plasma mass spectrometry with a total sample consumption system, Spectrochim. Acta B At. Spectrosc. 124 (2016) 99–108, https://doi.org/10.1016/j.sab.2016.08.018.
[45] C. Sánchez, C.P. Lienemann, J.L. Todolí, Metal and metalloid determination in bioethanol through inductively coupled plasma-optical emission spectroscopy, Spectrochim. Acta B At. Spectrosc. 115 (2016) 16–22, https://doi.org/10.1016/j.sab.2015.10.011.
[46] H. Habe, T. Shinbo, T. Yamamoto, S. Sato, H. Shimada, K. Sakaki, Chemical analysis of impurities in diverse bioethanol samples, J. Japan Pet. Inst. 56 (2013) 414–422, https://doi.org/10.1627/jpi.56.414.
[47] C. Sánchez, R. Sánchez, C.P. Lienemann, J.L. Todolí, ICP-MS spatial profiles in presence of ethanol and their application for the analysis of ethanol containing samples, J. Anal. At. Spectrom. 36 (2021) 2085–2096, https://doi.org/10.1039/D1JA00134E.